Inorg. Chem. **2005**, 44, 2177–2188

Inorganic Chemistry Article

Tb_4FeGe_8 Grown in Liquid Gallium: Trans–Cis Chains from the Distortion of a Planar Ge Square Net

Marina A. Zhuravleva,[†] Daniel Bilc,[‡] Robert J. Pcionek,[†] S. D. Mahanti,[‡] and Mercouri G. Kanatzidis*,[†]

Department of Chemistry and Department of Physics and Astronomy, Michigan State University,
East Lansing, Michigan 48824

Received August 31, 2004

The ternary germanide Tb_4FeGe_8 was obtained from Ga flux reactions. The crystal structure studied with single-crystal X-ray diffraction revealed the existence of an orthorhombic average substructure ($Cmcm$, $Z = 1$) with cell parameters $a = 4.1118(14)$ Å, $b = 15.844(5)$ Å, and $c = 3.9885(15)$ Å. The refinement [$I > 2\sigma(I)$] converged to final residuals R1/wR2 = 0.0363/0.0893. The average structure ($CeNiSi_2$-type) consists of a 3D [$Fe_{1/4}Ge_2$] framework where Ge atoms form a square net and Fe atoms reside alternatively above and below it with only $^1/_4$ occupation probability. X-ray and electron diffraction studies showed a modulation in the Ge net. The modulated structure was refined based on a 4-fold monoclinic supercell ($P2_1/n$) with parameters $a = 5.7315(11)$ Å, $b = 15.842(3)$ Å, $c = 11.438(2)$ Å, and $\beta = 91.724(4)°$ with $R_1/wR_2 = 0.0643/0.1735$ and uncovered a severe distortion of the Ge square net. The Ge atoms are displaced to form an array of cis–trans chains. The Ge–Ge distances within these chains are distinctively bonding, whereas those between the chains are nonbonding. Results of the electronic structure calculations and magnetic measurements are also reported. The structural distortions found in Tb_4FeGe_8 cast a doubt onto the correctness of many of the reported $REM_{1-x}Ge_2$ disordered compounds and call for reinvestigation.

Introduction

The populous $CeNiSi_2$ structure type[1] is represented in the realm of intermetallics by a rather large number of compounds.[2−4] Their general formula could be written as REM_xTt_2, where RE = rare-earth element, M = transition metal (Mn, Fe, Ni, Co, Cu, Ru, Rh, Re, Ir, Pd, Pt), and Tt = tetrelide (Si, Ge, Sn). The Tt atoms in this structure type define a flat square net. Even a compound with M = Li has been reported though it is not strictly isostructural.[5] Interestingly, most of these compounds are nonstoichiometric. A large variation of parameter x is found within a series of compounds with different RE or M element ($0 < x \leq 1$). At present, little is known about the nature of the vacancies on the M site. No direct correlation seemingly exists between x and the RE or M entity. Simple geometric considerations[6] also could not account for such variation of x. For example, in REM_xGe_2 and REM_xSn_2, x is increasing from Co to Ni to Fe although the atomic radii of these metals are very similar. In fact, all $REFe_xTt_2$ compounds are nonstoichiometric. The possibility of electronic reasons being responsible for the nonstoichiometry has been hinted.[7] The more wide-ranging trend in variation of x versus M, RE, and Tt elements has been outlined as follows:[8] for given RE and Tt, x increases with increasing atomic number of M, and for given RE and M, x generally decreases as the atomic number of Tt increases.

Because of the refractory nature of the constituting elements, most of the research in the RE−M−Tt system was

---

* To whom correspondence should be addressed. E-mail: kanatzid@cem.msu.edu.

[†] Department of Chemistry.

[‡] Department of Physics and Astronomy.

(1) Bodak, O. P.; Gladyshevskii, E. I. *Sov. Phys. Crystallogr.* **1970**, *14* (6), 859.

(2) Villars, P.; Calvert, L. D. *Pearson's Handbook of Crystallographic Data for Intermetallic Phases*; ASM International: Materials Park, OH, 1991.

(3) Szytula, A.; Leciejewicz, J. *Handbook of Crystal Structures and Magnetic Properties of Rare Earth Intermetallics*; CRC Press: Boca Raton, FL, 1994.

(4) Wang, X.-Z.; Lloret, B.; Ng, W. L.; Chevalier, B.; Etourneau, J.; Hagenmuller, P. *Rev. Chim. Min.* **1985**, *22*, 771.

(5) Pavlyuk, V. V.; Bodak, O. I.; Sobolev, A. N. *Sov. Phys. Crystallogr.* **1991**, *36*, 493.

(6) Francois, M.; Venturini, G.; Malaman, B.; Roques, B. *J. Less-Common Met.* **1990**, *160*, 197.

(7) Ijjaali, I.; Venturini, G.; Malaman, B. *J. Alloys Compd.* **1999**, *282*, 153.

(8) Nordiah, N. M.; Venturini, G.; Malaman, B.; Ressouche, E. *J. Alloys Compd.* **1998**, *265*, 77.

10.1021/ic0487878 CCC: $30.25

done using very high temperatures and polycrystalline powder samples. Single-crystal studies are available only for a limited number of compounds, for example, $NdFe_xGe_2$ [9] ($x = 0.45$) and $HoFe_xGe_2$ [9] ($x = 0.33$). In these cases, the shortened M−Ge bond distances as well as vacancies and unusual thermal ellipsoids found on the M atom point to possible superstructures. The single-crystal data for $REFe_{0.5}Si_2$ (RE = Dy, Ho)[10] also show highly perturbed thermal displacement parameters and partial occupancies characteristic of a superstructure, even though no superstructure reflections were observed. High-quality single crystals are hence particularly desirable in order to perform more in-depth investigations that could shed further light on the origin of the M vacancies.

Although hundreds of ternary rare-earth transition metal tetrelides have been reported over the past decades, mostly conventional methods were applied for their synthesis. An alternative synthetic route involves the use of molten metal (Ga, Al, Sn, etc.) as a flux. In cases when the flux is nonreactive, the metal solvent facilitates crystal growth[11,12] and does not incorporate into the final product. For silicides and germanides, molten Ga, for instance, may serve both as a reactive[13−17] and as a nonreactive solvent, even though the examples of the latter behavior are still scarce. Previously, we reported on the crystal growth of two families of silicides $RENiSi_3$ [18] and $RE_2Ni_{3+x}Si_{5-x}$ [19] from nonreactive Ga melts. Others employed the mixed-metal Zn/Ga flux in synthesis of $EuZn_2Si_2$ and $EuZn_2Ge_2$.[20] In the case of germanides, however, up until recently only Ga-containing compounds were reported from such Ga-flux reactions. Examples of the latter include the quaternary $RE_4FeGa_{12-x}Ge_x$,[14] $RE_{0.67}M_2Ga_{5+n-x}Ge_x$,[15] $REMGa_3Ge$,[16] $RE_3Ni_3Ga_8Ge_3$,[16] $RE_4Ni_3Ga_6Ge_4$,[21] and $RE_2MGa_9Ge_2$[21] and the ternary RE_3Ga_9Ge,[17] $Yb_3Ga_4Ge_6$,[22] $Yb_2Ga_4Ge_6$,[22] $RE_2Ga_2Ge_5$,[21] and La_3Ga_2Ge.[21] Here we present the Ga-flux synthesis and crystal growth of Tb_4FeGe_8 which adopts the $CeNiSi_2$ structure type. We show that the square net of Ge atoms found in the structure is only an artifact of the averaging effects of the $CeNiSi_2$ structure type. In fact, the Ge net is strongly modulated, and we successfully elucidated its structure using electron diffraction and X-ray crystallographic techniques. We also explored, through density functional calculations (DFT), the electronic reasons for this phenomenon. The results of X-ray and electron diffraction crystal structure determination of Tb_4FeGe_8 together with electronic structure calculations and magnetic properties are discussed.

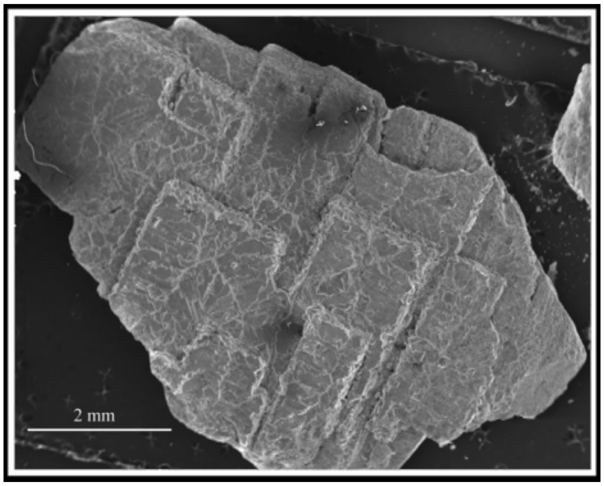

Figure 1. SEM image of a typical crystal of Tb_4FeGe_8 grown from liquid Ga.

Experimental Section

Synthesis. Tb_4FeGe_8 was synthesized in ~70% yield from a reaction containing 4, 1, 30, and 4 equiv of Tb, Fe, Ga, and Ge, respectively. The metals Tb (1 mm chips), Fe (300 mesh powder), Ga (3 mm shots), and Ge (polycrystalline, hand-ground), all of purity 99.9% and higher, CERAC Inc., were weighed in a glovebox under nitrogen atmosphere and loaded into an alumina crucible. The crucible was then sealed in a silica ampule under vacuum ($\sim 1 \times 10^{-4}$ Torr). The following heating profile was used for growing single crystals of Tb_4FeGe_8. The reaction mixture was heated to 1000 °C, held there for 5 h to obtain proper homogenization of the melt, cooled to 850 °C in 2 h, then held isothermally at 850 °C for 144 h, and finally cooled to 200 °C in 72 h. The reaction was taken out at 200 °C for hot filtration[14] to remove unreacted liquid Ga. Next, the reaction product was treated with a 3 M solution of I_2 in dimethylformamide (DMF) in order to isolate the crystals from the remaining flux. The final crystalline product was rinsed (under sonication) with water and DMF and subsequently dried with acetone and ether.

Scanning Electron Microscopy and Elemental Analysis. The elemental composition was studied by energy-dispersive spectroscopy (EDS) semiquantitative analysis on the scanning electron microscope (SEM) equipped with the NORAN Inc. EDS detector. The data acquisition was done at an acceleration voltage of 20 kV and a collection time of 30 s. The results obtained on a large number of crystals were averaged to obtain more accurate values of the atomic ratios. A typical crystal of Tb_4FeGe_8 grown in Ga flux is shown in Figure 1. A distinctive feature of this compound is the layered character of the crystals. The crystals are normally morphologically properly developed, platelike, well-faceted, and often featuring right angles. The surface of the crystals, as indicated by EDS analysis, tends to adhere to small particles of side products. Thus, the $FeGa_3$ and $Tb_2Ga_2Ge_5$ [21] phases were found to be locally present on the surface of the Tb_4FeGe_8 crystals. However, the EDS analysis taken on a freshly exposed cross section of the Tb_4FeGe_8

---

(9) Zheng, L.; Franzen, H. *J. Alloys Compd*. **1998**, *267*, 86.

(10) Paccard, L.; Paccard., D.; Allemand, J. *J. Less-Common Met.* **1990**, *161*, 295.

(11) Deitch, R. H. *Crystal Growth*; Pamplin, B. R., Ed.; Pergamon Press: Oxford and New York, 1975.

(12) Canfield, P. C.; Fisk, Z. *Philos. Mag. B* **1992**, *65* (6), 1117.

(13) Chen, X. Z.; Small, P.; Sportouch, S.; Zhuravleva, M.; Brazis, P.; Kannewurf, C. R.; Kanatzidis, M. G. *Chem. Mater*. **2000**, *12*, 2520.

(14) Zhuravleva, M. A.; Wang, X.; Schultz, A. J.; Bakas, T.; Kanatzidis, M. G. *Inorg. Chem*. **2002**, *41*, 6056.

(15) Zhuravleva, M. A.; Chen, X. Z.; Wang, X.; Schultz, A. J.; Ireland, J.; Kannewurf, C. K.; Kanatzidis, M. G. *Chem. Mater.* **2002**, *14,* 3066.

(16) Zhuravleva, M. A.; Pcionek, R. J.; Wang, X.; Schultz, A. J.; Kanatzidis, M. G. *Inorg. Chem.* **2003**, *42*, 6412.

(17) Zhuravleva, M. A.; Kanatzidis, M. G. *J. Solid State Chem.* **2003**, *173*, 280.

(18) Chen, X. Z.; Larson, P.; Sportouch, S.; Brazis, P.; Mahanti, S. D.; Kannewurf, C. R.; Kanatzidis, M. G. *Chem. Mater.* **1999**, *11*, 75.

(19) Zhuravleva, M. A.; Kanatzidis, M. G. *Z. Naturforsch.* **2003**, *58B*, 649.

(20) Grytsiv, A.; Kaczorowski, D.; Leithe-Jasper, A.; Rogl, P.; Godart, C.; Potel, M.; Noël, H. *J. Solid State Chem*. **2002**, *163*, 37.

(21) Zhuravleva, M. A. Doctoral Thesis Dissertation, Michigan State University, 2002.

(22) Zhuravleva, M. A.; Salvador, J.; Bilc, D.; Mahanti, S. D.; Ireland, J.; Kannewurf, C. R.; Kanatzidis, M. G. *Chem.—Eur. J.* **2004**, *10*, 3197.

crystals gave the composition "$Tb_4Fe_{1.24}Ge_{8.34}$". This is in good agreement with the formula obtained from the single-crystal X-ray diffraction refinement.[23]

Powder X-ray Diffraction. The X-ray powder diffraction (XRD) patterns of pulverized products were taken at room temperature on a CPS 120 INEL X-ray diffractometer (Cu Kα radiation) equipped with a position-sensitive detector. Experimental XRD patterns were then compared to that calculated from single-crystal data using the CERIUS^2 software package.[24] The yield of the Tb_4FeGe_8 phase was found to be maximal when the longer isothermal and cooling steps of the temperature variation profile were chosen. At the reaction conditions described above, the yield of the Tb_4FeGe_8 phase was 60−70%, according to the XRD. From the XRD pattern, the presence of Ge and ternary $Tb_2Ga_2Ge_5$ phase[21] was also evident. Additionally, traces of binary $FeGa_3$ and quaternary $Tb_4FeGa_{12-x}Ge_x$ [14] phases were observed during EDS elemental analysis but not in the XRD pattern. The latter two phases are therefore present in the amount less than 2%, below the detection limit of our powder X-ray diffraction method.

Single-Crystal X-ray Diffraction. The X-ray intensity data collection was carried out at room temperature on the Siemens Platform SMART[25] CCD diffractometer using a single crystal of dimensions $0.06 \times 0.04 \times 0.02$ mm^3 mounted on a glass fiber. A hemisphere of reflections (Mo Kα radiation, $\lambda = 0.710\,73$ Å) was acquired up to 56° in 2θ. The individual frames were measured using the ω-steps of 0.30° and an exposure time of 45 s per frame. The data acquisition and cell reduction were performed using SMART,[25] and further data reduction and integration were done with SAINTPLUS[25] software packages. The face-indexing procedure was used to analytically correct for absorption. The structure solution and refinement were done by direct methods on the basis of full-matrix least-squares on F^2 using SHELXTL software package. All atoms were refined anisotropically. The setting of the cell (substructure only) was standardized with the STRUCTURE TIDY program.[26]

Substructure Refinement. The initial cell reduction using SMART[25] readily gave an orthorhombic *C*-centered lattice with the following parameters: $a = 4.1118(14)$ Å, $b = 15.844(5)$ Å, and $c = 3.9885(13)$ Å. The systematic absences led to three possible space groups: $Cmc2_1$, *Cmcm*, and *Ama*2, of which the centrosymmetric one was proven to be correct during refinement. A total of four atomic positions (all of multiplicity 4*e*) were identified in the substructure of Tb_4FeGe_8. The site population of Fe was found to be substantially lower than full, while the rest of the atoms were found with ideal occupancies. Free refinement of the occupancy parameter of Fe at 4*e* showed it to be nearly 0.25, and therefore in the final refinement cycle it was constrained to exactly $^1/_4$. Short bond distances between Fe and some Ge atoms (2.147(3) Å) also validate the partial occupancy detected for Fe atoms. Additionally, the anisotropic displacement parameters U^{11} and U^{33} (directed along the *a*- and *c*-axis, respectively) of Ge(2) atoms were enlarged. The U^{33} parameters for the rest of atoms were on the contrary normal.

Superstructure Refinement. In Tb_4FeGe_8, the deficiency on the Fe site, shortened Fe−Ge bond distances, and unusual thermal displacement parameters raised suspicion for the existence of a superstructure. Even though the supercell could not be found during the cell reduction, further search for it was done with X-ray zone photographs. The photographs indicated the presence of the 4-fold monoclinic supercell with dimensions $(a^2 + c^2)^{1/2} \times b \times 2(a^2 + c^2)^{1/2}$, where *a*, *b*, and *c* are the parameters of the subcell. Given that the autoindexing algorithm of the SMART[25] software package was unable to carry out the indexing of the supercell (possibly due to the very weak superstructure reflections), a cell transformation matrix was imposed to convert the subcell to the 4-fold primitive supercell, $a' = 5.7315(11)$ Å, $b' = 15.842(3)$ Å, $c' = 11.438(2)$ Å, and $\beta = 91.724(4)°$. Intensity statistics suggested the $P2_1/n$ space group.[27] Subsequent refinement of the superstructure led to a reasonable convergence factor *R* of 0.0643 for $I > 2\sigma(I)$, although the Fourier difference map featured elevated (but not alarming) residual electron density peaks 5.424 and −6.753 e/Å^3.

A total of 14 general positions were found. Four of those were assigned to Tb, eight to Ge, and two to Fe atoms. Full occupancy was observed for all Tb and Ge sites, whereas the two Fe sites were found to be partially occupied (0.80 and 0.20 for Fe(1) and Fe(2), respectively) with a combined occupancy of 1. In the superstructure, all interatomic bond distances are regular, with the exception of the Fe(2) site, which exhibits shortened bonding contacts (1.989(17), 2.130(19), and 2.181(17) Å) to the neighboring Ge atoms. Owing to its low occupancy, the Fe(2) site that causes unreasonably close distances could be considered as a satellite peak, arising from either poor (weak) intensity data for the superstructure or the fact that a higher than 4-fold supercell may exist in Tb_4FeGe_8.

For the details of the data collection and structure refinement, see Table 1. The fractional atomic coordinates, isotropic thermal displacement parameters, and occupancies for the substructure and superstructure are presented in Table 2. The interatomic distances up to 3.5 Å for the substructures and superstructures are listed in Table 3. The anisotropic thermal displacement parameters for the substructures and superstructures are given in Table 4. Complete crystallographic information is contained in the Supporting Information section.

Transmission Electron Microscopy (TEM) and Electron Diffraction (ED). The TEM and ED studies were performed on a JEOL 100CX microscope. The electron beam was generated from the CeB_6 filament at accelerating voltage 120 kV. The samples were stable under the impact of the electron beam.

TEM Sample Preparation. Large, platelike, single crystals of Tb_4FeGe_8, normally over 10 mm^2 in area and up to 500 μm in thickness were selected. Because of the platelike habit of the crystals, only the [010] zone axis could be observed at zero tilt. The samples were hand-polished with sandpaper of subsequently increasing grit (1000−1500) to a thickness of approximately 200−300 μm. A core drill was then used to cut out a circular shape specimen 3 mm in diameter suitable for use in the TEM holder. As-prepared samples were electrochemically thinned using a Tenupol-3 twin-jet polishing unit equipped with an infrared detector. The electropolishing experiment was conducted at the temperature range from −35 to −40 °C with an applied potential of 30−35 V using a four-component acidic electrolyte.[28] The details of the thinning experiment have been described elsewhere.[21]

---

(23) This is despite complications caused by the partial overlap of the Kα-line of Fe (6.403 keV) and Lα-line of Tb (6.495 keV) in the X-ray emission spectra.

(24) *CERIUS^2*, version 1.6; Molecular Simulations Inc.: Cambridge, England, 1994.

(25) (a) *SMART*, version 5; Siemens Analytical X-ray Systems, Inc.: Madison, WI, 1998. (b) *SAINT*, version 4; Siemens Analytical X-ray Systems, Inc.: Madison, WI, 1994−1995.

(26) Gelato, L. M.; Parthé, E. *J. Appl. Crystallogr*. **1987**, *20*, 139.

(27) Even though the $P2_1/n$ is a nonstandard setting space group, it was meaningful to keep it unchanged in order to easily relate the superstructure to the substructure. The transformation to the standard setting ($P2_1/c$ space group) requires a different cell choice ($a = 5.732$ Å, $b = 15.842$ Å, $c = 12.638$ Å, $\beta = 115.23°$).

(28) Electrolyte composition (vol %): 10% H_2SO_4, 1%HF, 1.5% HNO_3, 87.5% CH_3OH.

Table 1. Crystal Data and Structure Refinement Details for Tb_4FeGe_8

empirical formula	(a) substructure of Tb_4FeGe_8	(b) superstructure of Tb_4FeGe_8
formula weight (g/mol)	1272.25	1272.25
temperature (K)	298(2)	298(2)
wavelength (Å)	0.71073	0.71073
crystal system	orthorhombic	monoclinic
space group	*Cmcm* (No. 63)	$P2_1/n$ (No. 14)
unit cell dimensions (Å)	$a = 4.1118(14)$	$a = 5.7315(11)$
	$b = 15.844(5)$	$b = 15.842(3)$; $\beta = 91.724(4)°$
	$c = 3.9885(13)$	$c = 11.438(2)$
volume (Å^3)	259.84(15)	1038.1(4)
Z	1	4
density (calcd) (g/cm^3)	8.130	8.141
absorption coefficient (mm^{-1})	50.850	50.913
F(000)	542	2168
crystal size (mm^3)	0.06 × 0.04 × 0.02	0.06 × 0.04 × 0.02
θ range for data collection (deg)	2.57−28.36	6.29−32.79
index ranges	$-5 \leq h \leq 3, -18 \leq k \leq 13, -3 \leq l \leq 5$	$-8 \leq h \leq 7, -17 \leq k \leq 23, -17 \leq l \leq 17$
reflections collected	502	5694
independent reflections	181 [$R_{int} = 0.0338$]	3367 [$R_{int} = 0.0448$]
completeness to $\theta = 28.36°$	85.4%	87.4%
refinement method	full-matrix least-squares on F^2	full-matrix least-squares on F^2
data/restraints/parameters	181/0/18	3367/0/118
goodness-of-fit on F^2	1.115	0.851
final *R* indices [$I > 2\sigma(I)$]^a	R1 = 0.0363, wR2 = 0.0893	R1 = 0.0643, wR2 = 0.1735
R indices (all data)	R1 = 0.0371, wR2 = 0.0898	R1 = 0.1457, wR2 = 0.2159
extinction coefficient	0.0096(14)	0.00051(6)
largest diff peak and hole (e/Å^3)	2.953 and −2.171	5.424 and −6.753^b

^{a} $R1 = \sum||F_o| - |F_c||/\sum|F_o|$; $wR2 = [\sum w\{|F_o| - |F_c|\}^2/\sum w|F_o|^2]^{1/2}$. ^{b} The high peak is located 0.72 Å from Tb(4), and the hole is at 0.84 Å from Tb(3).

Table 2. Atomic Coordinates, Equivalent Isotropic Displacement Parameters (Å^2 × 10^3) and Occupancies for the (a) Substructure and (b) Superstructure of Tb_4FeGe_8

atomic position	Wyckoff symbol	*x*	*y*	*z*	*U*(eq)^a	occ
			(a) Substructure			
Tb	4*c*	0	0.3966(1)	$^1/_4$	7(1)	1
Ge(1)	4*c*	0	0.0519(1)	$^1/_4$	10(1)	1
Ge(2)	4*c*	0	0.7525(2)	$^1/_4$	25(1)	1
Fe	4*c*	0	0.1972(5)	$^1/_4$	4(2)	$^1/_4$
			(b) Superstructure			
Tb(1)	4*e*	0.8756(5)	0.1029(1)	0.1884(2)	5(1)	1.0
Tb(2)	4*e*	0.3744(4)	0.1011(1)	0.4342(1)	5(1)	1.0
Tb(3)	4*e*	0.3757(4)	0.1025(1)	−0.0591(1)	6(1)	1.0
Tb(4)	4*e*	0.1250(4)	−0.1069(1)	0.3140(2)	6(1)	1.0
Ge(1)	4*e*	0.3746(10)	0.0464(2)	0.1881(4)	6(1)	1.0
Ge(2)	4*e*	0.8758(10)	0.0543(3)	−0.0615(3)	8(1)	1.0
Ge(3)	4*e*	0.6260(11)	−0.0572(2)	0.3134(4)	8(1)	1.0
Ge(4)	4*e*	0.8743(10)	0.0507(3)	0.4356(3)	9(1)	1.0
Ge(5)	4*e*	0.0946(6)	0.2487(3)	0.0532(2)	10(1)	1.0
Ge(6)	4*e*	0.6497(6)	0.2534(3)	0.0548(3)	12(1)	1.0
Ge(7)	4*e*	0.1082(7)	0.2541(2)	0.3221(3)	13(1)	1.0
Ge(8)	4*e*	0.6492(7)	0.2498(2)	0.3246(3)	16(1)	1.0
Fe(1)	4*e*	0.3753(10)	0.1977(2)	0.1872(5)	2(1)	0.8
Fe(2)	4*e*	0.8730(30)	0.1971(10)	0.4392(15)	6(3)	0.2

^{a} *U*(eq) is defined as one-third of the trace of the orthogonalized U^{ij} tensor.

Electronic Structure Calculations. Calculations were performed using the self-consistent full-potential linearized augmented plane wave method[29] within density functional theory[30] using the generalized gradient approximation of Perdew, Burke, and Ernzerhof[31] for the exchange and correlation potential. To avoid complications connected with presence of unfilled f-states of Tb atoms, the calculations were carried out on a hypothetical yttrium analogue. The following values of the atomic radii were taken: 2.0 au for Fe atoms, 2.05 au for Ge, and 2.3 au for Y atoms, where au is the atomic unit (0.529 Å). Convergence of the self-consistent iterations was performed to within 0.0001 Ry with a cutoff of −6.0 Ry between the valence and the core states for 9 and 32 *k* points[32] inside the Brillouin zones of superstructures and substructures, respectively. Scalar relativistic corrections were included, and the spin−orbit interaction was incorporated using a second variational procedure.[33] The calculations were performed using the WIEN2K program.[34]

Magnetic Measurements. Magnetic susceptibility studies were carried out on single-crystal and polycrystalline samples of Tb_4FeGe_8. Single crystals of Tb_4FeGe_8 were selected manually and polished with sandpaper of increasing fineness (1000−1500) to remove possible surface impurities. The measurements were carried out in the temperature range 2−400 K with an applied magnetic field of 500 G. Measurements of magnetization as a function of field (up to ±5 T) were also performed. Both susceptibility and magnetization data acquisition included isotropic measurements where the pulverized sample was used, as well as anisotropic, for which the single crystal was placed with the *b*-axis parallel or perpendicular to the direction of the external magnetic field (H_{ex}).

Results and Discussion

Reaction Chemistry. Large single crystals of Tb_4FeGe_8 could be grown from molten Ga; see Figure 1. The ability of liquid Ga to enable crystal growth is thus quite remarkable,

---

[29] Singh, D. *Planewaves, Pseudopotentials, and the LAPW Method*; Kluwer Academic: Boston, MA, 1994.

[30] (a) Hohenberg, P.; Kohn, W. *Phys. Rev.* **1964**, *136B*, 864. (b) Kohn, W.; Sham, L. *Phys. Rev.* **1965**, *140*, A1133.

[31] Perdew, J. P.; Burke, K.; Ernzerhof, M. *Phys. Rev. Lett.* **1996**, *77*, 3865.

[32] This particular number of *k* points was chosen in order to have approximately the same density of *k* points inside the Brillouin zones.

[33] Koelling, D. D.; Harmon, B. *J. Phys. C: Solid State Phys.* **1980**, *13*, 6147.

[34] Blaha, P. K.; Schwarz, G.; Madsen, D.; Kvasnicka, Luitz, J. *WIEN2K, an Augmented Plane Wave + Local Orbitals Program for Calculating Crystal Properties*; Schwarz, Karlheinz, Ed.; Vienna University of Technology: Vienna, Austria, 2001.

Table 3. Bond Lengths [Å] for the (a) Substructure and (b) Superstructure of Tb_4FeGe_8

(a) Substructure

bond	distance	multiplicity	bond	distance	multiplicity	bond	distance	multiplicity
Tb−Ge(1)	2.9778(10)	×4	Tb−Fe	3.228(4)	×4	Ge(2)−Fe	2.235(3)	×2
Tb−Ge(2)	3.073(2)	×2	Ge(1)−Fe	2.302(9)	×1	Ge(2)−Ge(2)	2.8653(7)	×4
Tb−Ge(2)	3.092(2)	×2	Ge(1)−Ge(1)	2.586(3)	×2	Fe−Ge(2)	2.147(3)	×2
Tb−Fe	3.159(8)	×1	Ge(1)−Tb	2.9778(10)	×4	Fe−Ge(2)	2.235(3)	×2
Tb−Ge(1)	3.2063(19)	×2	Ge(2)−Fe	2.147(3)	×2			

(b) Superstructure

bond	distance	bond	distance	bond	distance	bond	distance
Tb(1)−Ge(4)	2.946(4)	Tb(2)−Ge(8)	3.117(4)	Tb(3)−Ge(2)	3.205(4)	Ge(3)−Ge(4)	2.604(8)
Tb(1)−Ge(2)	2.961(4)	Tb(2)−Ge(7)	3.118(4)	Tb(4)−Ge(3)	2.966(7)	Ge(4)−Fe(2)	2.320(17)
Tb(1)−Ge(1)	2.997(7)	Tb(2)−Ge(4)	3.187(4)	Tb(4)−Ge(3)	2.978(7)	Ge(4)−Ge(4)	2.587(9)
Tb(1)−Ge(1)	3.008(7)	Tb(2)−Fe(1)	3.213(5)	Tb(4)−Ge(4)	2.999(4)	Ge(5)−Fe(2)	2.259(19)
Tb(1)−Ge(5)	3.070(4)	Tb(2)−Ge(3)	3.226(4)	Tb(4)−Ge(2)	3.005(4)	Ge(5)−Fe(1)	2.333(6)
Tb(1)−Ge(6)	3.095(5)	Tb(2)−Fe(2)	3.235(18)	Tb(4)−Fe(1)	3.096(3)	Ge(5)−Ge(8)	2.643(3)
Tb(1)−Ge(8)	3.106(4)	Tb(3)−Ge(1)	2.963(5)	Tb(4)−Ge(7)	3.123(4)	Ge(6)−Fe(2)	2.181(17)
Tb(1)−Ge(7)	3.119(4)	Tb(3)−Ge(2)	2.964(7)	Tb(4)−Ge(6)	3.126(5)	Ge(6)−Fe(1)	2.385(7)
Tb(1)−Fe(2)	3.234(17)	Tb(3)−Ge(2)	2.967(7)	Tb(4)−Ge(5)	3.158(4)	Ge(6)−Ge(5)	2.552(3)
Tb(1)−Fe(1)	3.234(6)	Tb(3)−Ge(8)	2.971(4)	Tb(4)−Ge(8)	3.160(4)	Ge(6)−Ge(7)	2.668(3)
Tb(1)−Ge(2)	3.235(4)	Tb(3)−Ge(7)	2.983(4)	Tb(4)−Fe(2)	3.163(18)	Ge(7)−Fe(2)	2.130(19)
Tb(1)−Fe(1)	3.236(6)	Tb(3)−Ge(3)	2.996(5)	Tb(4)−Ge(1)	3.184(4)	Ge(7)−Fe(1)	2.380(7)
Tb(2)−Ge(1)	2.946(4)	Tb(3)−Ge(5)	3.120(5)	Tb(4)−Ge(4)	3.218(4)	Ge(7)−Ge(8)	2.632(4)
Tb(2)−Ge(3)	2.969(5)	Tb(3)−Ge(6)	3.123(5)	Ge(1)−Fe(1)	2.397(4)	Ge(8)−Fe(2)	1.989(17)
Tb(2)−Ge(4)	2.975(7)	Tb(3)−Fe(2)	3.175(16)	Ge(1)−Ge(2)	2.564(8)	Ge(8)−Fe(1)	2.339(6)
Tb(2)−Ge(6)	2.996(5)	Tb(3)−Fe(1)	3.195(5)	Ge(1)−Ge(3)	2.589(7)		
Tb(2)−Ge(5)	3.000(5)	Tb(3)−Ge(1)	3.149(4)	Ge(2)−Ge(2)	2.616(9)		

Table 4. Anisotropic Displacement Parameters ($Å^2 \times 10^3$) for the (a) Substructure and (b) Superstructure of Tb_4FeGe_8[a]

atom	U^{11}	U^{22}	U^{33}	U^{23}	U^{13}	U^{12}
(a) Substructure						
Tb	8(1)	9(1)	2(1)	0	0	0
Ge(1)	9(1)	20(1)	1(1)	0	0	0
Ge(2)	30(1)	10(2)	34(1)	0	0	0
Fe	5(3)	7(5)	0(3)	0	0	0
(b) Superstructure						
Tb(1)	6(1)	7(1)	2(1)	0(1)	0(1)	0(1)
Tb(2)	7(1)	7(1)	2(1)	0(1)	0(1)	0(1)
Tb(3)	6(1)	8(1)	3(1)	0(1)	0(1)	−1(1)
Tb(4)	6(1)	8(1)	4(1)	1(1)	0(1)	0(1)
Ge(1)	6(1)	9(1)	3(1)	0(2)	−1(1)	1(2)
Ge(2)	7(2)	15(2)	2(2)	−1(1)	1(1)	−2(2)
Ge(3)	8(1)	13(1)	4(1)	0(2)	−1(1)	−1(3)
Ge(4)	5(2)	19(2)	4(2)	0(1)	−2(1)	0(2)
Ge(5)	6(1)	12(2)	14(1)	−2(1)	0(1)	−2(2)
Ge(6)	4(1)	14(2)	17(1)	0(2)	1(1)	1(2)
Ge(7)	18(1)	9(1)	12(1)	−2(2)	−7(1)	1(2)
Ge(8)	24(2)	13(1)	11(1)	−4(1)	13(1)	−4(2)

[a] The anisotropic displacement factor exponent takes the form $-2\pi^2[h^2a^{*2}U^{11} + ... + 2hka^*b^*U^{12}]$.

considering that compounds of this type (rare-earth transition metal tetrelides) are usually produced in polycrystalline form. The Tb_4FeGe_8 seems to be the first representative of the $CeNiSi_2$ structure type to be grown from liquid Ga. $TbFe_{0.42}Ge_2$ has been previously obtained by conventional methods and characterized by powder diffraction.[6] It is also interesting to see the sequence of phase formation, which occurs in the quaternary Tb−Fe−Ga−Ge system under flux conditions. Longer reaction times give mainly Tb_4FeGe_8. Shorter temperature profiles resulted in the formation of the quaternary $Tb_4FeGa_{12-x}Ge_x$ [14] phase. It appears that initially the $Tb_4FeGa_{12-x}Ge_x$ phase is produced, which then decomposes to the Ga-free Tb_4FeGe_8 along with the Fe-free phase $Tb_2Ga_2Ge_5$. The $Tb_4FeGa_{12-x}Ge_x$ could be regarded as only a kinetically stable product.

Crystal Structure. (a) Average Structure. The structure of Tb_4FeGe_8 (or $TbFe_{0.25}Ge_2$, for easier comparison) is related to a well-known $CeNiSi_2$ structure type.[1] Although the structure of the latter does not exhibit any deficiency on the corresponding Ni site, a large number of isotypic compounds are nonstoichiometric and show a wide homogeneity range.[2,6] In particular, $TbFe_xTt_2$ crystallizing in $CeNiSi_2$ structure type are now obtained with Tt = Si, Ge, and Sn. As mentioned above, parameter x in these compounds seems to be commensurate with the atomic number of the tetrelide. For instance, single-crystal data give x to be $^1/_2$ for Tt = Si,[10] $^1/_4$ for Tt = Ge, and $^1/_8$ for Tt = Sn.[35] The only stoichiometric compound known in the $TbFe_xTt_2$ family is $TbFeSi_2$. It crystallizes in $NdRuSi_2$-type,[36] monoclinically distorted low-temperature polymorphic modification of $CeNiSi_2$-type. Interestingly, many compounds in the REM_xGe_2 [6] family have been reported with $x = {}^1/_4$ or close to it. These include $GdFe_{0.25}Ge_2$, $LuFe_{0.23}Ge_2$, $GdCo_{0.24}Ge_2$, $LuCo_{0.27}Ge_2$, $ErCu_{0.25}Ge_2$, $GdMn_{0.26}Ge_2$, $HoMn_{0.25}Ge_2$, $ErMn_{0.27}Ge_2$, $TmMn_{0.25}Ge_2$, $LuMn_{0.27}Ge_2$, $GdRe_{0.25}Ge_2$, $HoRe_{0.25}Ge_2$, $GdRu_{0.23}Ge_2$, $HoRu_{0.27}Ge_2$, $LuRu_{0.25}Ge_2$, $GdRh_{0.24}Ge_2$, $HoRh_{0.28}Ge_2$, and $LuRh_{0.23}Ge_2$. Similarly, $x = {}^1/_2$ is more common for silicides, for example, $REFe_{0.5}Si_2$ (RE = Tb, Dy, Ho, Er, Lu),[10] $TmLi_{0.5}Ge_2$,[5] and $NdFe_{0.45}Ge_2$.[9] Although it could be coincidental, it is also possible that it indicates the existence of different fold superstructures: 2-fold, 4-fold, and 8-fold (or even higher multiples) for $CeNiSi_2$-type silicides, germanides, and stannides, respectively.

The substructure of Tb_4FeGe_8 viewed down the c-axis is shown in Figure 2A. No bonds were drawn to Tb atoms to better emphasize the three-dimensional $[Fe_{1/4}Ge_2]$ framework

---

(35) Zhuravleva, M. A.; Kanatzidis, M. G. Work in progress.

(36) Cenzual, K.; Gladyshevskii, R. E.; Parthé, E. *Acta Crystallogr., Sect. C* **1992**, *48*, 225.

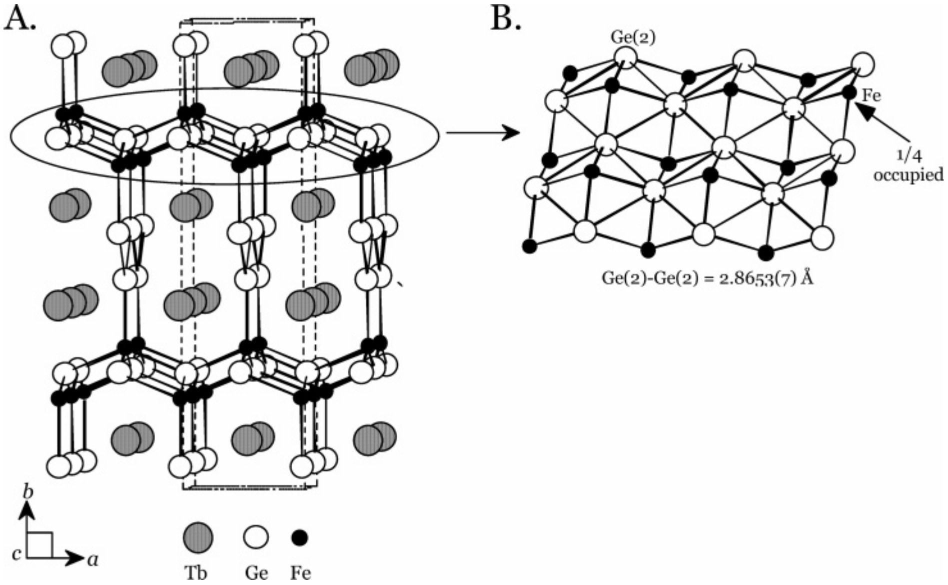

Figure 2. (A) Projection of the substructure (*Cmcm*) of Tb_4FeGe_8 onto the *ab*-plane. For clarity, the bonds to Tb atoms are not drawn. (B) A fragment of the $[Fe_{1/4}Ge(2)]$ puckered layer viewed approximately down the *b*-axis. Open circles, Ge atoms; large black circles, Tb atoms.

and its channels. The channels stretch along the *c*-axis, and each of them accommodates a pair of Tb atoms. If broken down into fragments, the $[Fe_{1/4}Ge_2]$ framework could be thought of as constructed of infinite Ge(1) zigzag chains and $[Fe_{1/4}Ge(2)]$-puckered layers. The Ge(1) zigzag chains extend along the *c*-axis with the plane of the chain being parallel to the *bc* plane.

The $[Fe_{1/4}Ge(2)_2]$ slab is shown in Figure 2B, and it deserves special attention as the apparent disorder reveals itself in this particular layer. The slab contains a planar square net defined by Ge(2) atoms. The Ge(2)−Ge(2) bond distances in the layer are 2.8653(7) Å. On one hand, these are quite large compared to normal Ge−Ge bonds or the sum of covalent radii (2.44 Å);[37,38] however, they are much shorter than those found in the related, stoichiometric $LaNiGe_2$ [39] compound (3.020 Å). Above and below the Ge(2) square net are Fe atoms located in a puckered manner. In such a puckered layer, the Fe atoms are only partially occupied (25%). This allows for unrealistically shortened Fe−Ge(2) bond distances of 2.147(3) Å to occur in this layer. The next closest Fe−Ge(2) contact is at 2.235(3) Å, and it is yet considerably shorter than the corresponding Ni−Ge bonds in $LaNiGe_2$ [39] (2.4055(9) and 2.4360(10) Å). Note that the only difference between the stoichiometric $LaNiGe_2$ and nonstoichiometric Tb_4FeGe_8 ($TbFe_{0.25}Ge_2$) is the size of the Ge openings in the square net. In the former case, the larger 3.02 × 3.02 Å^2 squares easily accommodate 100% of Ni atoms; while for Tb_4FeGe_8, the smaller size (2.87 × 2.87 Å^2) Ge openings are not able to accommodate all Fe atoms without generating uncomfortably short bond distances.

(b) Superstructure. The unacceptably short Ge−Fe distances caused us to seek rational explanations such as the possibility of an artifact originating from averaging a large modulated long-range superstructure over a small unit cell. The first indication for superstructure in Tb_4FeGe_8 came from X-ray [010] zone photographs taken on the CCD diffractometer with the exposure time of 3000 s, Figure 3. Later, the superstructure was confirmed by single-crystal electron diffraction; see below. In the X-ray zone photograph, only four reflections with indices ±2 0 ±1 (marked by arrows) correspond to a subcell; see Figure 3. The remaining reflections belong to a supercell and were indexed in the monoclinic primitive lattice with dimensions $(a^2 + c^2)^{1/2} \times b \times 2(a^2 + c^2)^{1/2}$ where *a*, *b*, and *c* are the substructure parameters. No superstructure reflections were seen along the *b**-axis in the *hk*0 or 0*kl* zone photographs indicating that there is no modulation along the *b*-axis. It is not surprising that the supercell reflections could not be initially observed during the data collection (45 s), as their intensity is very weak even

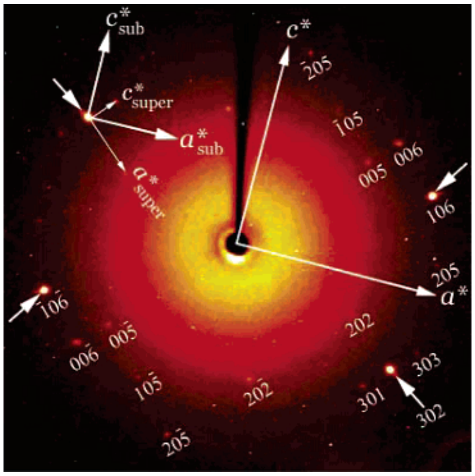

Figure 3. The [*h*0*l*] x-ray diffraction zone photograph for Tb_4FeGe_8 taken with the exposure time of 3000 s. The ±2 0 ±1 reflections of the subcell are pointed out with arrows. The Bragg spots are indexed in the $(a^2 + c^2)^{1/2} \times b \times 2(a^2 + c^2)^{1/2}$ supercell.

---

(37) Wulfsberg, G. In *Inorganic Chemistry*; University Science Books: Sausalito, CA, 2000; p 32.

(38) Pauling, L. In *The Nature of the Chemical Bond*, 3rd ed.; Cornell University Press: Ithaca, NY, 1960; p 410.

(39) Prosperio, D. M.; Chacon, G.; Zheng, C. *Chem. Mater.* **1998**, *10*, 1268.

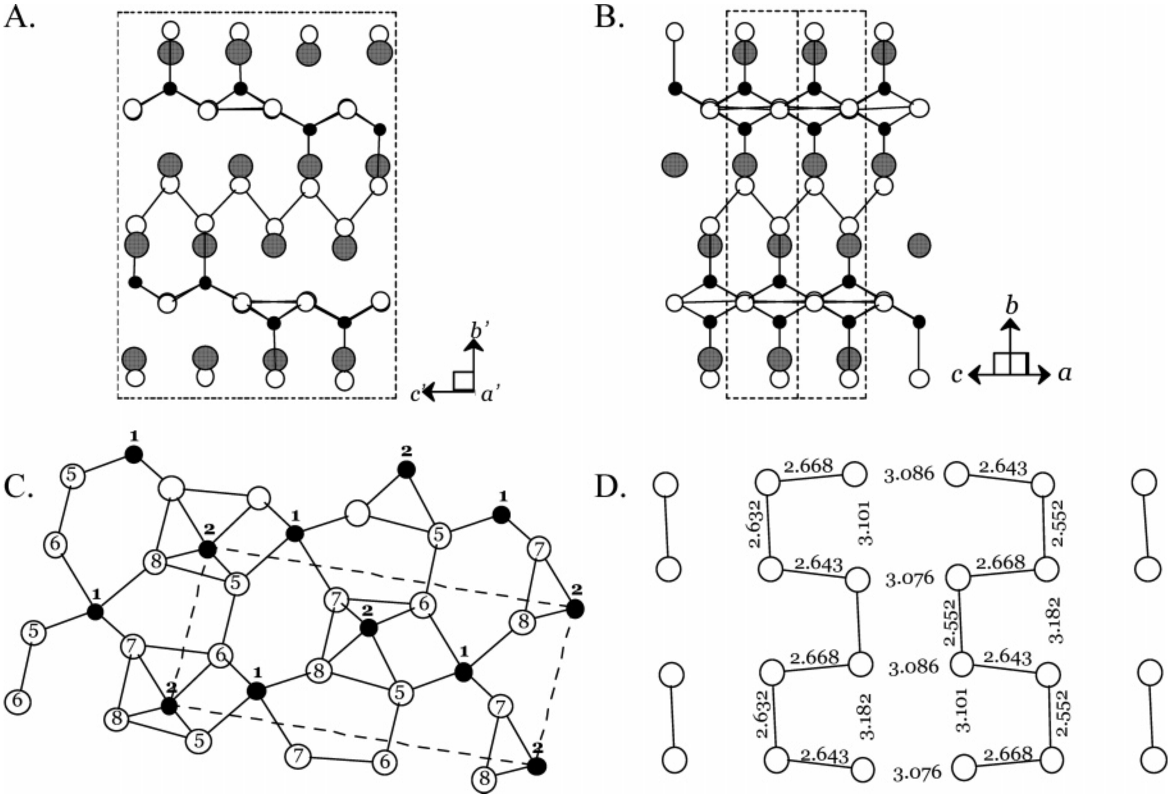

Figure 4. Side-by-side representation of the long-range structure (A) and average structure (B) of Tb_4FeGe_8. (C) A single Fe−Ge puckered layer found in the superstructure of Tb_4FeGe_8 viewed approximately down the *b*-axis. The numbering for the corresponding crystallographic sites is enclosed in the circle and given on the side for Ge and Fe, respectively. The unit cell is shown with a dashed line. (D) The modulated structure of the Ge square net resolved into parallel cis−trans chains. The Ge−Ge bonds were drawn within the cutoff distance of 3 Å. Open circles, Ge atoms; large black circles, Tb atoms.

in zone photographs taken at long exposure times. Nevertheless, it was possible to obtain a reasonable refinement of the superstructure and resolve the nature of the modulation in Tb_4FeGe_8. The refinement results provide unique insight in understanding the substructure−superstructure relationship and the driving force for superstructure formation.

A drawing of the 4-fold superstructure is depicted in Figure 4A. For the sake of consistency, all atoms are drawn in the same manner as in the substructure. The substructure (viewed along the diagonal) is given for reference in Figure 4B. The severe distortion of the Ge square lattice is striking. The main dissimilarity between the two lies in the distortion of the Ge net and ordering of Fe atoms in the Fe−Ge layer. A single Fe−Ge layer of the superstructure is given in Figure 4C. Four crystallographically distinct Ge atoms (Ge(5)−Ge(8))[40] and two Fe atoms (Fe(1) and Fe(2)) are involved in its construction.

The distortion breaks the square net of Ge atoms into arrays of parallel cis−trans chains, Figure 4D. Interestingly, a monoclinic distortion of the $CeNiSi_2$-type has also been observed for the compounds of $NdRuSi_2$ [36] structure type; however, it bears only a distant resemblance[41] with that occurring in Tb_4FeGe_8. The distances within the cis−trans chains range from 2.552(3) to 2.668(3) Å, while those between the chains are much larger and span a range of 3.076−3.182 Å. In contrast to Ge−Ge distances in the square net, the Ge atoms of 1D zigzag chain are conserved (2.564(8)−2.616(9) Å in the superstructure versus 2.586(3) Å in the substructure).

As a result of the displacement of Ge atoms from their average position in the square lattice, openings of different shapes and sizes are generated, Figure 4D. The Fe atoms effectively cap only the larger squarelike openings where Ge−Ge distances are in the range 3.076−3.182 Å. Not surprisingly, these compare very well with the 3.02 Å × 3.02 Å openings in the stoichiometric $LaNiGe_2$. Every fourth opening in the Ge net is large enough to effectively accommodate Fe atoms in capping positions, in accord with the $^1/_4$ occupancy of Fe in the substructure.

The superstructure forms due to a distortion of the square net of Ge which brings about the differentiation between the Ge−Ge bond distances and produces parallel cis−trans chains. It follows that the energy of the crystal lattice is lowered when a group of weak Ge−Ge bonds (in the ideal net) are exchanged for a set of strongly bonding and nonbonding interactions (in the distorted net). Because of the severity of the distortion, we believe the main driving force to be electronic in nature. The accommodation of only $^1/_4$ of Fe atoms in the capping position is due possibly to size effects, but electronic factors cannot be ruled out. With only $^1/_4$ of Fe atoms present, a closer orbital overlap is

---

(40) Four other Ge atoms (Ge(1)−Ge(4)) are correspondingly part of the Ge-only zigzag chains.

(41) In $NdRuSi_2$, the monoclinic distortion breaks down the square net of Si atoms into an array of zigzag chains; the bonding within the chains is even stronger, and the separation between the chains is even larger than that for Tb_4FeGe_8.

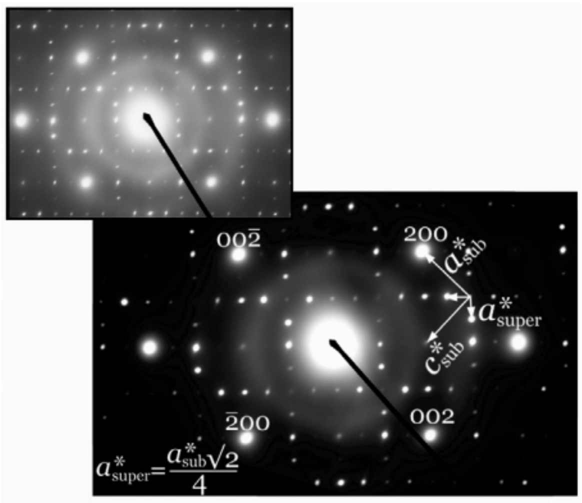

Figure 5. The [010] zone axis SAED pattern from a single crystal of Tb_4FeGe_8. Selected subcell reflections are indexed. The corresponding vectors of the reciprocal subcell and supercell are denoted as a^*_{sub}, c^*_{sub} and a^*_{super}, c^*_{super}, respectively.

achieved between Fe and Ge, which is revealed in the shorter Fe−Ge bond distances of 2.359 Å on average (compare to Ge−Ni distances of 2.4055(9) and 2.4360(10) Å in the related $LaNiGe_2$). The overall effect is such that by removing $^3/_4$ of the Fe atoms from the hypothetical "$TbFeGe_2$" and allowing the Ge lattice to relax, energy stabilization is gained through enhanced bonding in the Fe−Ge puckered layer. This phenomenon of modulations and distortion in square nets driven by electronic factors is known in tellurium-based systems where an ideal net of Te atoms distorts to chains or oligomeric fragments depending on electron count per Te atom.[42] On the basis of the work reported here, it would appear that this effect is more general and operates in nets made of other main group elements.

Single-Crystal Electron Diffraction. The partial occupancy on the Fe(1) and Fe(2) atoms and the short bond distances generated between the Fe(2) atoms and Ge atoms could possibly indicate the presence of even higher order superstructure. Interestingly, electron diffraction does evidence an even higher order superstructure for Tb_4FeGe_8; see Figure 5. The selected area electron diffraction pattern taken along the [010] zone axis on a single-crystal sample of Tb_4FeGe_8 shows the presence of an 8-fold superstructure. The modulation occurs, as in the previous case, along both diagonal directions of the orthorhombic cell, and the a'' and c'' supercell parameters are $2(a^2 + c^2)^{1/2} \times 2(a^2 + c^2)^{1/2}$. This additional weaker modulation may be due to ordering of the Fe atoms in the net or further modulation along the Ge chains. Unfortunately, because of the lack of a sufficient number of reflections in the X-ray data corresponding to this supercell, it was impossible to reliably refine the 8-fold superstructure from the X-ray intensity data. As was shown above, the 4-fold superstructure provides information regarding the distortion that is completely masked up in the substructure. Therefore, the refined 4-fold superstructure may be a good compromise between the misleadingly averaged substructure and possibly correct but not well-resolved 8-fold superstructure in Tb_4FeGe_8.

Electronic Structure. As mentioned above, this type of distortion most likely originates from the nature of electronic structure of this compound. To explore this further, theoretical electronic calculations were performed. It is well-known that LDA and GGA approximations within density functional theory cannot adequately treat partially filled f-shells. To avoid this problem, we have carried out our calculations for the hypothetical Y_4FeGe_8 compound, since Y is devoid of any f-electrons and both Y and Tb ions are trivalent. Furthermore, because most of the structural distortions occur in the Fe−Ge network, we expect our electronic structure calculations for Y_4FeGe_8 to give us a proper physical understanding of the underlying driving mechanism in Tb_4FeGe_8. Single-crystal structure refinement gives two types of Fe sites in the Y_4FeGe_8 monoclinic superstructure, one of which is 80% occupied and the other is only 20% occupied. For rigorous calculations of such disorder, one has to choose an even larger unit cell than that of the superstructure. This was clearly beyond the scope of the present ab initio calculations. Instead, we decided to work with the refined superstructure and assume the Fe(1) site to be fully occupied while neglecting the low occupancy of the Fe(2) site.[43]

The goal of the electronic structure calculations was threefold: (1) to verify that the superstructure is energetically more stable than the substructure; (2) to assess why a stoichiometric $Tb_4Fe_4Ge_8$ ($TbFeGe_2$) has not been experimentally observed; and (3) to get further insight into Ge net distortion. First, the results of the theoretical electronic calculations show that there is a substantial difference in total energy (E_{tot}) between the substructures and superstructures. The modulated structure is predicted to have lower energy by 1.04 eV/fu(Y_4FeGe_8) and thus be more energetically favorable. Second, to further study the stability of the observed nonstoichiometric Y_4FeGe_8 phase versus the fully stoichiometric $Y_4Fe_4Ge_8$, we calculated their cohesive energies, E_{coh}. The E_{coh} is defined as the difference between E_{tot} of the solid and E_{tot} of the constituent parts of the solid. The values of E_{coh} are given by the following equations:

$$E_{coh}(\text{Y}_4\text{FeGe}_8\text{ superstructure}) = E_{tot}(\text{Y}_4\text{FeGe}_8\text{ superstructure}) - E_{tot}(\text{Y}_4\text{Ge}_8\text{ superstructure}) - E_{tot}(\text{Fe atom in bulk})$$

$$E_{coh}(\text{Y}_4\text{Fe}_4\text{Ge}_8\text{ substructure}) = E_{tot}(\text{Y}_4\text{Fe}_4\text{Ge}_8\text{ substructure}) - E_{tot}(\text{Y}_4\text{Ge}_8\text{ substructure}) - 4E_{tot}(\text{Fe atom in bulk})$$

These values for the Y_4FeGe_8 superstructure and $Y_4Fe_4Ge_8$

---

(42) Kanatzidis M. G.; Patschke, R. *Phys. Chem. Chem. Phys.* **2002**, *4*, 3266.

(43) Additionally, to be able to compare the results of the calculations for the smaller orthorhombic average substructure with the larger monoclinic superstructure and account for the partial Fe occupancy, we had to present the substructure in the larger cell with dimensions $(a^2 + c^2)^{1/2} \times b \times 2(a^2 + c^2)^{1/2}$, similar to the Y_4FeGe_8 monoclinic superstructure. Note that the only difference between this larger subcell construct and the actual monoclinic supercell is that the Ge(2) square lattice in the former is not distorted.

substructure are −2.53 and +2.52 eV respectively, showing that the Y_4FeGe_8 phase is a stable phase (negative E_{coh}), whereas the $Y_4Fe_4Ge_8$ phase is not a stable phase. The results are again consistent with the observation that the $Y_4Fe_4Ge_8$ phase has not been seen experimentally.

Third, to elucidate the driving force behind the superstructure formation, we closely examined the energetic effects brought about by the distortion of the Ge(2) square net. For this, we compared E_{tot} of the Fe-free hypothetical Y_4Ge_8 superstructure and Y_4Ge_8 substructure. The Y_4Ge_8 substructure has a lower energy than that of Y_4Ge_8 superstructure by 0.81 eV/f.u.(Y_4Ge_8).[44] Consequently, in the absence of Fe, a distortion in the Ge net does not seem to be energetically favorable. The presence of the transition metal thus has to be responsible for the destabilization and distortion of the square net.

Density of states (DOS) analysis for the Y_4FeGe_8 superstructure shows metallic behavior with a value of ∼30 states/{(eV)(4[Y_4FeGe_8])} at the Fermi energy, E_F (Figure 6A). The largest contribution to the DOS at E_F are Fe d-states (∼1.5 states/(eV•atom)), which are not fully occupied (Figure 6B). The Ge(1) p-states (Ge in zigzag chains) and Ge(2) p-states (Ge in distorted square nets) span a broad range between −5 and 10 eV, contributing ∼0.1 states/(eV•atom) to the DOS at E_F. The Ge s-states are located between −11 and −6 eV (Figure 6C,D), indicating a bandwidth comparable to the bandwidths of the p-bands. The difference between occupied Ge(1) and Ge(2) p-states is that the former states are mostly located below −1.5 eV; therefore, these states are better stabilized in energy than the Ge(2) p-states. The Y d-states are mostly empty centered about 5 eV with a value of ∼0.2 states/(eV•atom) of DOS at E_F (Figure 6E). Between −5 and 0 eV, the Ge(1) and Ge(2) p-states hybridize with the d-states of Fe and Y atoms. These will have implications in the long-range interaction between the rare-earth moments because the rare-earth f-states have strongest interactions with their s- and d-states (see discussions following the magnetic properties).

Magnetic Properties. The temperature dependence of the molar magnetic susceptibility ($\chi^{\perp}_{m}$) and reciprocal molar susceptibility $(\chi^{\perp}_{m})^{-1}$ for the external magnetic field (H_{ex}) oriented perpendicular to the crystallographic *b*-axis of a single crystal of Tb_4FeGe_8 is shown in Figure 7A (left panel). The low-temperature region of $\chi^{\perp}_{m}$ is characterized with the maximum centered at $T_{max} \sim 19$ K; see Figure 7A (right panel). The system thus appears to undergo an antiferromagnetic transition below T_{max}. The Néel temperature $T_N = 20.4$ K was determined in a series of susceptibility measurements performed in fields of 100−2000 G. As the temperature increases above 50 K, the $(\chi^{\perp}_{m})^{-1}$ increases linearly with temperature. The behavior of $(\chi^{\perp}_{m})^{-1}$ versus *T* obeys the Curie−Weiss law at high *T*. The intercept with the temperature axis gives the Weiss constant ($\Theta^{\perp}$), which has a small positive value of +3.8 K (indicating ferromagnetic coupling between the magnetic moments). The effective magnetic moment ($\mu^{\perp}_{eff}$) obtained from the slope of the line is 9.68μ_B and is very close to the value for the free Tb^{3+} ion[45] (9.72μ_B).

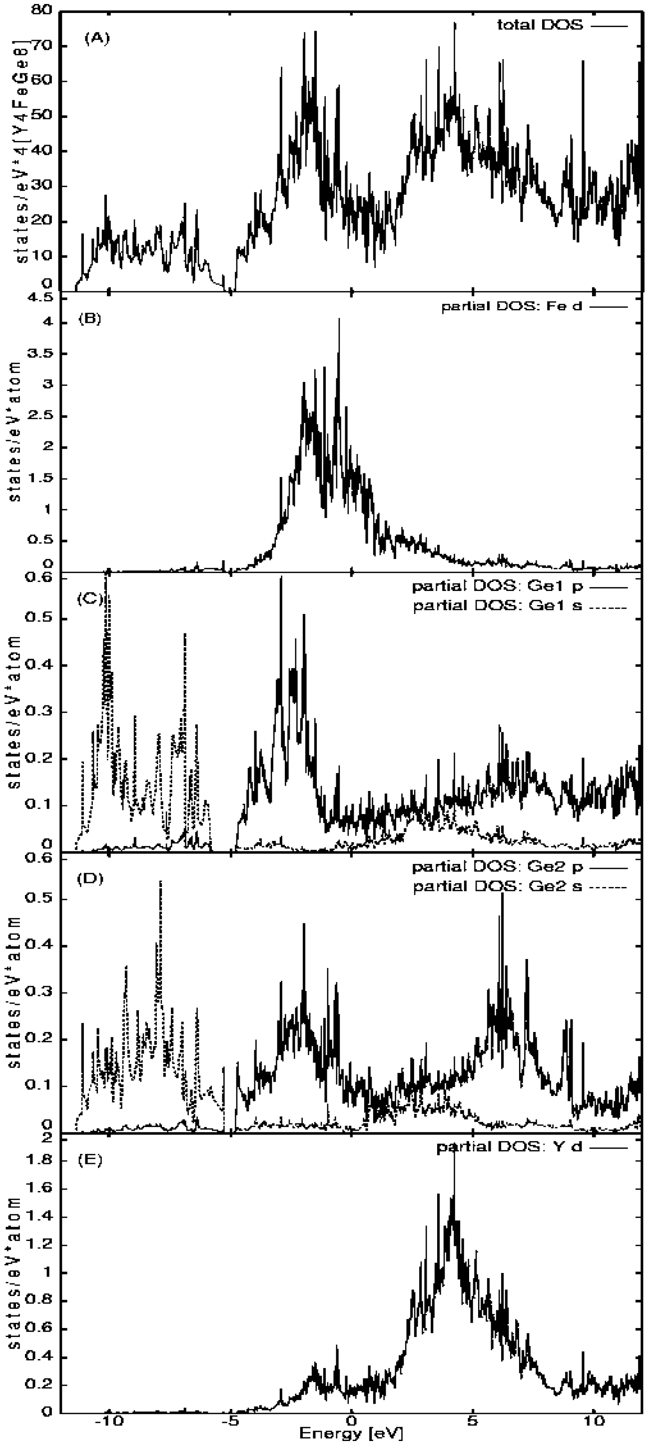

Figure 6. Density of states for Y_4FeGe_8 (superstructure model).

Interestingly, if the external field H_{ex} is directed parallel to the *b*-axis the magnetic response is quite different; see Figure 7B (left panel). First of all, no T_{max} is observed up to the temperature of ∼2.5 K. Instead, the $\chi^{\parallel}_{m}$ continues to rise as could be seen in the expanded area of the low-temperature

---

(44) This result, however, does not exclude the possible existence of other Y_4Ge_8 superstructures with lower energy than that of Y_4Ge_8 substructure.

(45) The effective magnetic moment could be obtained by the formula $\mu_{eff} = g_J[J(J + 1)]^{1/2}$, where g_J is a Landé factor and *J* is a total angular momentum of the Tb^{3+} ion.

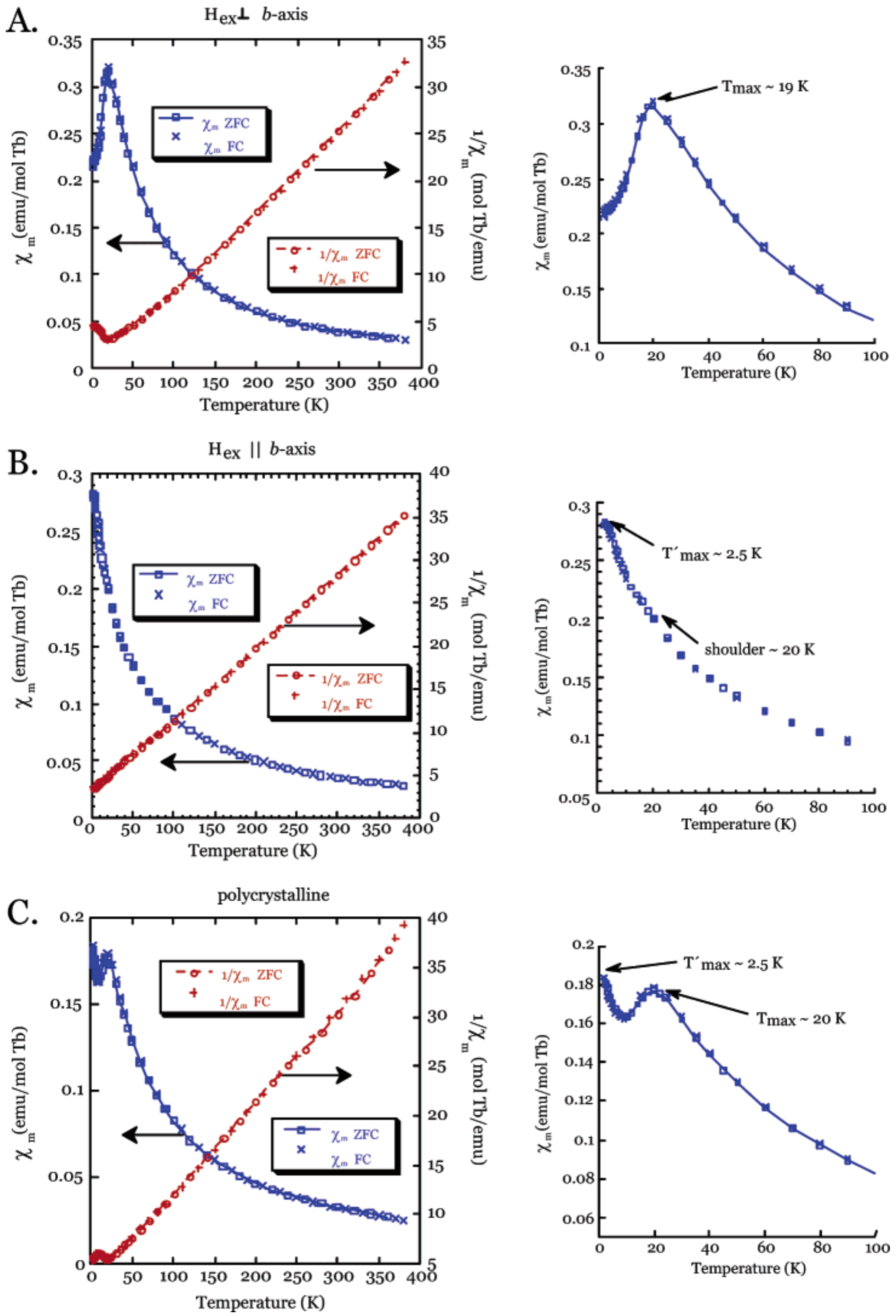

Figure 7. Molar magnetic susceptibility and inverse susceptibility for a single crystal of Tb_4FeGe_8 (A and B) oriented with the *b*-axis perpendicular (A) to the external magnetic field or parallel (B) to the external magnetic field and for a polycrystalline sample of Tb_4FeGe_8 (C). The expanded area of low-temperature susceptibility data is given on the right.

region in Figure 7B (right panel). The pronounced maximum, which is clearly seen at ∼20 K in the $\chi^{\perp}_{m}-T$ plot, is revealed only as a weak shoulder in the $\chi^{||}_{m}-T$ graph.[46] Moreover, the onset of an additional upturn on the $\chi^{||}_{m}-T$ plot appears at $T'_{max} \sim 2.5$ K. At high temperatures $(\chi^{||}_{m})^{-1}$ shows Curie−Weiss behavior with $\Theta^{||} = -36$ K indicating antiferromagnetic coupling between the moments. The experimental value of $\mu^{||}_{eff}$ calculated from the slope of $(\chi^{||}_{m})^{-1}-T$ is in excellent agreement with the theoretical μ_{eff} for the free Tb^{3+} ion. Thus, it is clear that in both cases it is the Tb^{3+} moment which is responsible for the magnetic response. The Fe atoms are essentially nonmagnetic. Similar nonmagnetic character of Fe atoms was observed in the intermetallic compounds $RE_4Fe_{2+x}Al_{7-x}Si_8$[47] (RE = Ce, Pr, Nd, Sm) and $Tb_4FeGa_{12-x}Ge_x$.[14] The dramatically different response be-

---

(46) There may be two reasons for observing a shoulder in the $\chi-T$ plot when the external field is parallel to the *b*-axis. First, it could be due to a small misalignment of the crystal with respect to external magnetic field, given that the crystal is positioned in the field manually using its well-defined morphology. Alternatively, because of the lower symmetry associated with the structural distortions, the effective spin Hamiltonian could have terms which couple component of spin parallel to the *b*-axis (*y*-axis) with those parallel to the *x* and *z* axes.

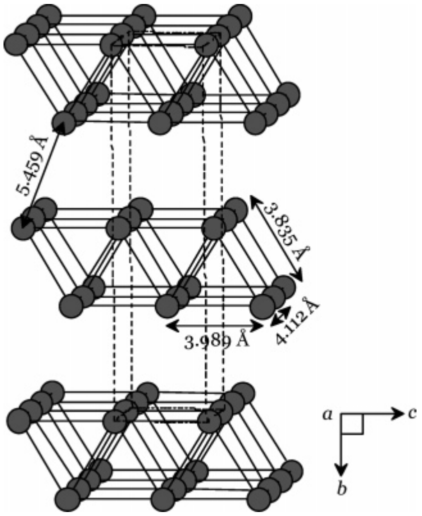

Figure 8. The Tb-only sublattice in the structure of Tb_4FeGe_8. The unit cell is drawn with dashed lines.

tween $\chi^{||}_m$ and $\chi^{\perp}_m$ clearly signifies that the interaction between the Tb moments is highly anisotropic and complex with competing ferromagnetic and antiferromagnetic couplings.

From a geometrical point of view, the origin of the two different types of interactions may lie in the packing of Tb atoms, which mediates the exchange interaction between the Tb ions. The Tb-only framework could be considered as consisting of $[Tb_6]$ trigonal prisms condensed into 2D layers via face-sharing. These Tb layers extend infinitely in the *ac*-plane and stack along the *b*-axis with an intralayer separation of ~5.5 Å; see Figure 8. The nearest Tb−Tb bond contacts occur at 3.835, 3.988, and 4.112 Å. These distances are quite close to the sum of single-bonded metallic radii 3.55 Å for Tb[48] (CN = 12) and therefore may contain a certain amount of covalent character. The next nearest Tb−Tb contact is at 5.459 Å, which could only be regarded as nonbonding. Consequently, in the Tb-only framework, the bonding interactions in $[Tb_6]$ prisms are comparable in both rectangular faces (*ac*-plane) and pseudotrigonal faces (*bc*-plane). Interestingly, in compounds with a pure trigonal arrangement of Tb atoms and comparable Tb−Tb distances of ~4 Å, such as $Tb_{0.67}Ni_2Ga_{5-x}Ge_x$,[15] the values of T_{max} (~3 K) are very close to T'_{max} (~2.5 K) observed in Tb_4FeGe_8. Similarly, the Tb compounds containing only an orthorhombic arrangement of Tb atoms such as $Tb_2Ni_{3+x}Si_{5-x}$ [19] (again with similar Tb−Tb distances of ~4 Å) are characterized with T_{max} (~15 K) comparable to T_{max} (~20 K) for Tb_4FeGe_8. This serves as an additional indication that interactions in Tb_4FeGe_8 are of one type if the moments are oriented on the *ac*-plane and of different type when the moments are oriented on the *bc*- or *ab*- plane.

This is a classic example of competing long-range anisotropic interactions and can be understood by looking at the calculated electronic structure. Since the system is metallic, the interaction between the Tb moments is primarily of long-range Ruderman−Kittel−Kasuya−Yoshida type that is oscillatory in nature (both ferromagnetic and antiferromagnetic type coupling depending on the distance between two RE ions). Also the band structure is anisotropic and therefore one expects this interaction to be anisotropic. Finally, the Tb^{3+} ion has orbital magnetic moment, and additional anisotropy may arise due to this. It will be interesting to compare these results with a spin-only case, which is the case for Gd^{3+} compounds. We have previously observed such anisotropy due to angular momentum in virtually every heavy RE analogue of $RE_{0.67}Ni_2Ga_{5-x}Ge_x$ [15] but Gd, which has no contribution from the orbital magnetic momentum to its total momentum.

The isotropic susceptibility of the polycrystalline sample is expected to reflect the average contribution from both antiferromagnetic transitions. Indeed, isotropic magnetic susceptibility measurements performed on polycrystalline samples of Tb_4FeGe_8, Figure 7C (left panel), clearly show two ordering transitions to an antiferromagnetic state. The inspection of the expanded low-temperature region of χ_m^{iso} and $(\chi_m^{iso})^{-1}$, see Figure 7C (right panel), shows that the first transition is centered at ~2.5 K and the next one is at ~20 K, just as in the case of $\chi_m^{||}$ and $\chi_m^{\perp}$, respectively. The μ_{eff} obtained from the slope of the χ^{iso}_m-T plot gives the value of $9.61\mu_B$, close to that calculated for the free Tb^{3+} ion. The field-dependence measurements show no saturation up to fields of 5 T, with the maximal magnetic moment ranging from $1.8\mu_B$ to $3\mu_B$ depending on the orientation. An analogous situation was observed in a number of Tb-containing intermetallic compounds including $Tb_2Ni_{3+x}Si_{5-x}$,[19] $TbNiGa_3Ge$,[16] and $TbAl_{3-x}Ge_x$.[49]

Concluding Remarks

Large crystals of Tb_4FeGe_8, a new derivative of the $CeNiSi_2$ structure type, have been obtained in reactions involving excess liquid Ga. This is also a primary example of the nonreactive behavior of the Ga flux in the quaternary RE−M−Ga−Ge system.

The quality of the grown crystals facilitated more detailed studies of the structural and magnetic properties of this new compound. An interesting structural peculiarity is the presence of a “perfect” square net of Ge atoms and a “disorder” observed in the $[Fe_{1/4}Ge]$ plane, which is revealed in the Fe site vacancies and the shortened Fe−Ge bond distances, which we have now shown to be an artifact of the existence of a 4-fold to 8-fold supercell, with the modulation propagating along the diagonal of the orthorhombic subcell. The strong modulation is due to a distortion in the Ge square net in the structure.

Total energy calculations suggest an energy lowering of 1.04 eV/f.u.(Y_4FeGe_8) due to distortions in the Ge network in the presence of Fe atoms. The theoretical calculations also suggest that stoichiometric $Y_4Fe_4Ge_8$ compounds may not be stable. The magnetism in Tb_4FeGe_8 is due to the free

---

(47) Sieve, B.; Sportouch, S.; Chen, X, Z.; Cowen, J. A.; Brazis, P.; Kannewurf, C. R.; Papaefthymiou, V.; Kanatzidis, M. G. *Chem. Mater.* **2001**, *13*, 273.

(48) Pauling, L. In *The Nature of the Chemical Bond*, 3rd ed.; Cornell University Press: Ithaca, NY, 1960; p 403.

(49) Zhuravleva, M. A.; Rangan, K. K.; Lane, M.; Brazis, P.; Kannewurf, C. R.; Kanatzidis, M. G. *J. Alloys Compd.* **2001**, *316*, 137.

Tb^{3+} ion, while the Fe atoms in the structure are nonmagnetic. The compound exhibits two antiferromagnetic ordering events that depend on the direction of the magnetic field with Néel temperatures T_N of 2.5 and 20 K. Surprisingly, the higher T_N direction gives a small ferromagnetic Curie–Weiss Θ, whereas the one associated with low T_N gives a large antiferromagnetic Curie–Weiss Θ. These observations indicate anisotropic competing (ferromagnetic and antiferromagnetic) interactions between Tb moments. This is consistent with the calculated electronic structure of this compound.

The structural findings for Tb_4FeGe_8 we report here cast doubt onto the correctness of the reported $REM_{1-x}Ge_2$ disordered compounds and call for reinvestigation. A large number of the already reported structures of $REM_{1-x}Ge_2$ compounds were solved in the subcell setting with M atom disorder; however, their refinement details bear lucid indications of the superstructure.

Acknowledgment. Financial support from the Department of Energy (Grant No. DE-FG02-99ER45793) is gratefully acknowledged. This work made use of the SEM and TEM facilities of the Center for Advanced Microscopy at Michigan State University. We are indebted to Prof. M. A. Crimp of the Department of Chemical Engineering and Materials Science at Michigan State University for providing the electropolishing unit and for fruitful discussions. A generous gift of rare earth elements from Treibacher Industrie AG is gratefully acknowledged.

Note Added after ASAP: This manuscript was released ASAP on March 8, 2005, with an incomplete Acknowledgment. The correct version was published on March 10, 2005.

Supporting Information Available: Tables of crystallographic details, atomic coordinates, isotropic and anisotropic thermal displacement parameters for all atoms, and interatomic distances and angles for Tb_4FeGe_8 substructures and superstructures (in cif format). This material is available free of charge via the Internet at http://pubs.acs.org.

IC0487878